Phloem Loading through Plasmodesmata: A Biophysical Analysis[1][OPEN]

Jean Comtet,[a] Robert Turgeon,[b] and Abraham D. Stroock[a,c,2]

[a]School of Chemical and Biomolecular Engineering, Cornell University, Ithaca, New York 14853
[b]Plant Biology Section, Cornell University, Ithaca, New York 14853
[c]Kavli Institute at Cornell for Nanoscale Science, Cornell University, Ithaca, New York 14853

ORCID IDs: 0000-0003-2389-3879 (J.C.); 0000-0002-6019-6741 (R.T.); 0000-0002-8145-9977 (A.D.S.).

In many species, Suc en route out of the leaf migrates from photosynthetically active mesophyll cells into the phloem down its concentration gradient via plasmodesmata, i.e. symplastically. In some of these plants, the process is entirely passive, but in others phloem Suc is actively converted into larger sugars, raffinose and stachyose, and segregated (trapped), thus raising total phloem sugar concentration to a level higher than in the mesophyll. Questions remain regarding the mechanisms and selective advantages conferred by both of these symplastic-loading processes. Here, we present an integrated model—including local and global transport and kinetics of polymerization—for passive and active symplastic loading. We also propose a physical model of transport through the plasmodesmata. With these models, we predict that (1) relative to passive loading, polymerization of Suc in the phloem, even in the absence of segregation, lowers the sugar content in the leaf required to achieve a given export rate and accelerates export for a given concentration of Suc in the mesophyll and (2) segregation of oligomers and the inverted gradient of total sugar content can be achieved for physiologically reasonable parameter values, but even higher export rates can be accessed in scenarios in which polymers are allowed to diffuse back into the mesophyll. We discuss these predictions in relation to further studies aimed at the clarification of loading mechanisms, fitness of active and passive symplastic loading, and potential targets for engineering improved rates of export.

Vascular plants export sugars and other nutrients from leaves through a living vascular tissue, the phloem. This transport process drives photosynthetic products to remote tissues (sinks) for growth and storage, coupling synthesis, and intercellular transport processes in the leaves and sink tissues to global, hydraulic transport through the phloem sieve tubes and xylem vessels. Significant uncertainties remain regarding the structure, chemistry, and transport phenomena governing these processes (Knoblauch and Peters, 2010; Turgeon, 2010a, 2010b). Improved models of export will inform our understanding of whole-plant physiology and open opportunities to engineer sugar concentrations and transport processes to improve growth and yield (Schroeder et al., 2013; Giraldo et al., 2014). Insights into these transport processes may also suggest ways to design efficient synthetic systems to control chemical processes (Stroock et al., 2014; Comtet et al., 2017).

Particular outstanding questions relate to the mechanisms by which plants transfer Suc, and in some cases sugar alcohols, from the photosynthetically active mesophyll to the transport phloem (phloem loading) in the subset of species in which this loading step occurs symplastically, i.e. through the open channels of plasmodesmata (Fu et al., 2011; Zhang et al., 2014; Fig. 1A). In most symplastic loaders, there is no buildup of sugars in the phloem, as shown in Figure 1B; this distribution of sugars suggests passive transfer from mesophyll to phloem, as postulated by Münch (1930). In a second symplastic loading mechanism, Suc passes from mesophyll cells into bundle sheath cells and from the bundle sheath into specialized phloem companion cells in the minor veins known as intermediary cells through specialized plasmodesmata (Fig. 1A). In the intermediary cells, the Suc is converted, in an energetically active polymerization process, to raffinose family oligosaccharides (RFOs; principally raffinose and stachyose). Transfer of RFOs back into the mesophyll does not appear to occur, and one observes elevated total concentrations of sugars in the phloem relative to the mesophyll (Fig. 1B; Voitsekhovskaja et al., 2006; Haritatos et al., 1996; Fisher 1986). This inversion of the total concentration gradient of sugars depends on the polymerization reaction (McCaskill and Turgeon, 2007)

[1] J.C. and A.D.S. acknowledge support from the Air Force Office of Scientific Research (FA9550-15-1-0052) and the Camille Dreyfus Teacher-Scholar Awards Program. R.T. acknowledges support from the National Science Foundation-Integrative Organismal Systems (1354718).

[2] Address correspondence to ads10@cornell.edu.

The author responsible for distribution of materials integral to the findings presented in this article in accordance with the policy described in the Instructions for Authors (www.plantphysiol.org) is: Abraham D. Strook (ads10@cornell.edu).

A.D.S. and R.T. conceived the project; J.C. performed the modeling work with input from R.T. and A.D.S.; J.C., R.T., and A.D.S. analyzed and interpreted results and wrote the article.

[OPEN] Articles can be viewed without a subscription.

www.plantphysiol.org/cgi/doi/10.1104/pp.16.01041

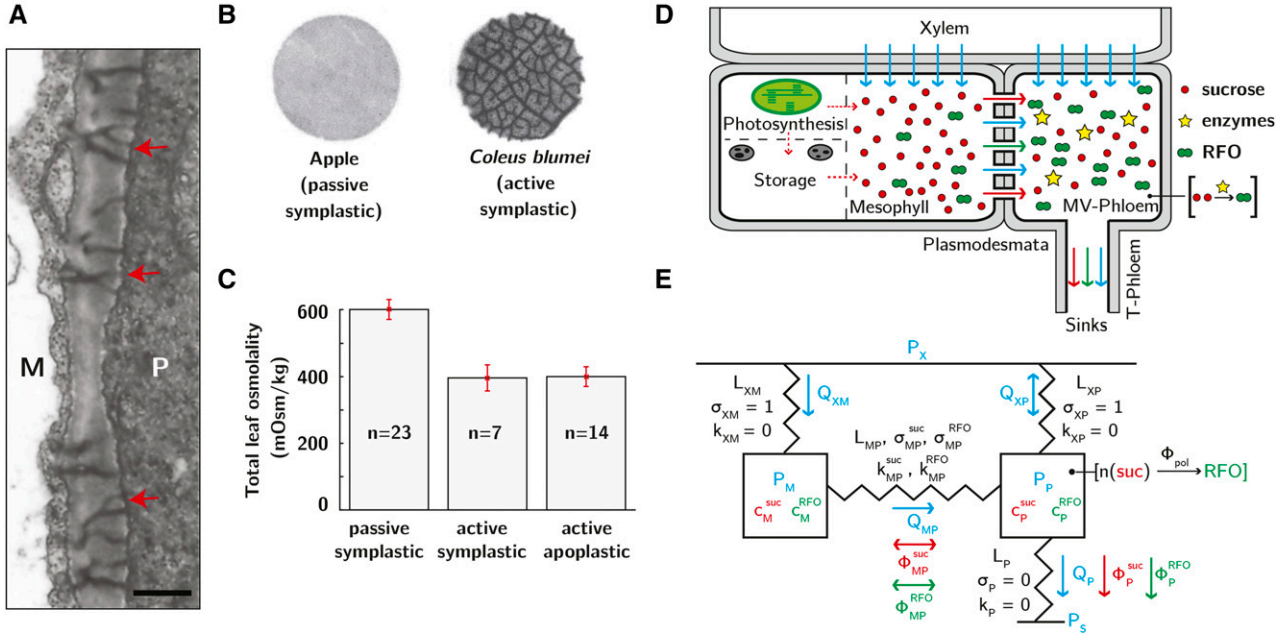

Figure 1. Overview of phloem loading and global model of symplastic phloem transport. A, Cross-sectional view of mesophyll/phloem (M/P) interface of a mature *Cucumis melo* leaf, showing plasmodesmata with the secondary branching pattern that is characteristic of active symplastic loaders (red arrowheads). Bar = 250 nm. Adapted from Volk et al. (1996). B, Autoradiographs of leaf discs from apple (*Malus domestica*), a passive symplastic loader, and *Coleus blumei*, an active symplastic loader. Abraded discs were incubated in [^{14}C]Suc, washed, freeze dried, and pressed against x-ray film. Minor veins are apparent in *C. blumei*, but not apple discs. Discs are 8 mm diameter. Adapted from Turgeon (2010a) and Rennie and Turgeon (2009). C, Total leaf osmolality in passive and active symplastic and apoplastic loading species. Error bars are SE; derived from Rennie and Turgeon (2009). D, Model for water and sugar transport in active and passive symplastic loaders. Carbon fixed from CO_2 is used to synthesize Suc (red circles) or is transiently stored as starch. Suc passes through plasmodesmata down a concentration gradient from the mesophyll to the phloem. In active symplastic loaders, most of the Suc entering the phloem is polymerized into RFO (green) by an enzymatic process (yellow stars). Depending on the plasmodesmatal properties, some of the RFO can diffuse back to the mesophyll cells. Suc and RFO are then exported via bulk flow in the transport phloem. E, Circuit diagram of model in D. Hydraulic interfaces are characterized by hydraulic permeabilities (L [m s^{-1} Pa^{-1}]) and reflection coefficients (σ [−]) ($\sigma = 1$ for osmotic membranes); the plasmodesmata interface is further characterized by a diffusive mass transfer coefficient (k [m s^{-1}]). Volumetric fluxes of water (Q [m s^{-1}], blue arrows) and molar fluxes of solute (ϕ [mole m^{-2} s^{-1}], red arrows) pass through the circuit from the xylem at pressure, P_X [Pa] to tissue sinks for the sugars at a pressure, P_S [Pa]. In the MV-phloem, n Suc are polymerized to form one RFO at a rate ϕ_{pol} [mole m^{-2} s^{-1}]. See Table I for values of all parameters used.

and correlates with lower concentration of sugars in the mesophyll, and hence in the whole leaf, relative to plants that load passively (Rennie and Turgeon, 2009; Fig. 1C). In these two characteristics (inverted total concentration gradient of sugars and lower total sugar content in leaves), active symplastic loaders, also known as polymer trappers, match the characteristics of apoplastic loaders in which photoassimilate is actively pumped into the phloem (Fig. 1C; Haritatos et al., 1996; Voitsekhovskaja et al., 2006; Rennie and Turgeon, 2009). In this paper, we refer to RFO accumulation in the phloem as "segregation" and the elevated total concentration of sugars in the phloem relative to the mesophyll as "gradient inversion."

The observation of strong segregation of sugars in the phloem (Fig. 1B) and low levels of whole-leaf osmolarity (Fig. 1C) in polymer trap plants provokes a number of questions. First, what mechanisms permit passive transport of Suc through these apparently open pores from mesophyll to minor vein phloem, while simultaneously preventing the passage of larger RFOs in the opposite direction? One possibility is that the plasmodesmata in question are very narrow, allowing Suc to pass via diffusion (Haritatos and Turgeon, 1995; Liesche and Schulz, 2013; Turgeon and Gowan, 1990) or advection (Dölger et al., 2014; Voitsekhovskaja et al., 2006) while inhibiting RFO backflow on the basis of steric selectivity. However, coupling of local plasmodesmatal dynamics with whole-plant transport of water and sugars and the kinetics of polymerization has so far been neglected. A second question is raised by segregation: How can phloem osmolarity be higher than in the mesophyll given that polymerization reactions reduce the number of osmotically active molecules in the phloem sap? Finally, a more general question: How do the rates of symplastic loading, convective export, and polymerization influence sugar segregation and translocation rates?

Only a few models of phloem transport consider loading mechanisms and distinguish between mesophyll and phloem (Dölger et al., 2014; Lacointe and Minchin, 2008; Thompson and Holbrook, 2003). Other simplified modeling approaches (Jensen et al., 2011, 2012; Jensen and Zwieniecki, 2013) have given insight into phloem traits at the plant scale but avoid the question of phloem loading by considering a fixed hydrostatic pressure in the phloem. In this article, we introduce a global model of water and sugar transport in symplastic loading species with explicit kinetics of polymerization (Fig. 1, D and E). We then consider the transport properties of plasmodesmata, including the relative importance of diffusion and advection, and determine how long-distance transport is affected by the segregation of Suc polymers in the phloem. These analyses provide new insights into the nature of symplastic loading mechanisms and the adaptive advantages they confer.

RESULTS

A Globally Coupled Model of Symplastic Loading with Polymerization

Figure 1D is a schematic cross section of a leaf minor vein in symplastic loaders (either passive or active; electron micrograph in Supplemental Fig. S1) presenting the hypothesized transport processes: Photosynthetic products (Fig. 1D, red circles; Suc in all plants and also sugar alcohols in some) diffuse and advect through plasmodesmata (cross-sectional view in Figure 1A) down their concentration gradient from the mesophyll (site of synthesis) to the phloem (site of advective evacuation). Suc is then polymerized into RFOs in the phloem (green double circles in Figure 1D). Elevated osmolarity in the mesophyll and phloem recruits water from the xylem (Fig. 1D, blue arrows) to drive convection along this pathway. Water and sugars are subsequently exported by advection through the transport phloem (T-phloem) to sinks (Fig. 1D, blue and red downward arrows, respectively).

Figure 1E presents a circuit representation of steady fluxes of water (Q_i [m s^{-1}], blue arrows) and sugars (ϕ_i [mole m^{-2} s^{-1}], red arrows) from xylem to the mesophyll (Q_{XM}) and to the MV-phloem (Q_{XP}), from mesophyll to the MV-phloem ($Q_{MP}; \phi_{MP}^{suc};\ \phi_{MP}^{RFO}$), and through the phloem to sink tissues ($Q_P;\ \phi_P^{suc};\ \phi_P^{RFO}$). All fluxes are defined with respect to the exchange surface area of MV-phloem through which Suc loading occurs. The zig-zag black lines in Figure 1E represent available paths for water and sugar transfer. Each path presents a hydraulic conductance (L [m s^{-1} Pa^{-1}]) for water flow. The interface of the mesophyll and phloem with the xylem is a perfect osmotic membrane that excludes passage of sugars by either advection (reflection coefficient, $\sigma_{XM} = \sigma_{XP} = 1$) or diffusion [diffusive mass transfer coefficient, $k_{XM} = k_{XP} = 0$ (m s^{-1})] (Katchalsky and Curran, 1965). The plasmodesmatal interface between the mesophyll and phloem partially reflects sugars ($0 \leq \sigma_{MP} \leq 1$) and allows for diffusive transfer of sugars ($k_{MP} \geq 0$); we explore details of plasmodesmatal transport processes in Figure 2. The transport phloem allows water flow and free advective transfer of sugars ($\sigma_P = 0$), and we neglect diffusion of sugars ($k_P = 0$). We consider Michaelis-Menten kinetics for polymerization of n Suc into one RFO at rate $\phi_{pol} = \frac{\phi_{pol}^{MM} c_P^{suc}}{K_M + c_P^{suc}}$ with ϕ_{pol}^{MM} the maximal polymerization rate and K_M the Michaelis-Menten constant. With $\phi_{pol}^{MM} = 0$, the system models passive symplastic loading. See "Materials and Methods" and Supplemental Information S1 for details.

Nondimensional Parameters That Characterize Loading

In the model of active symplastic loading described above (Fig. 1, D and E), diffusive loading of Suc from mesophyll to phloem and advective export of sugars within the phloem occur simultaneously. We expect that the relative magnitudes of these fluxes should play an important role in defining distinct regimes of the predicted behavior, i.e. advection-limited (greater diffusive Suc loading compared to advective export of sugars) versus diffusion-limited (minimal diffusive loading of Suc compared to advective export of sugars). Here, we identify the characteristic magnitude of these rates and normalize the global advection of sugars within the transport phloem by the diffusive component of transport through plasmodesmata. We call the resulting nondimensional ratio the flushing number (f) and show, in the following sections and in a separate study (Comtet et al., 2017), that it provides a useful parameterization of the predicted behavior, even when we consider both advective and diffusive transport inside the plasmodesmata (see Supplemental Information S2).

First, we identify the characteristic net driving force, ΔP_c, for water flow from leaf to sink as the mesophyll osmotic pressure minus the negative pressure difference between leaf xylem and the unloading zone in the transport phloem:

$$\Delta P_c = RTc_M^{suc} + P_X - P_S \ . \tag{1}$$

Second, analysis of the hydraulic network gives a total conductance for the leaf in series with the transport phloem:

$$L_{tot} = \frac{1}{\frac{1}{L_{leaf}} + \frac{1}{L_P}} \tag{2}$$

where $L_{leaf} = 1/(1/L_{XM} + 1/L_{MP}) + L_{XP}$ is the effective conductance of the leaf (L_{XP} is in parallel with L_{XM} and L_{MP}, which are in series). We assume here that water can enter the leaf from xylem to mesophyll, or from xylem to phloem. Together, Equations 1 and 2 define the characteristic water flux through the phloem:

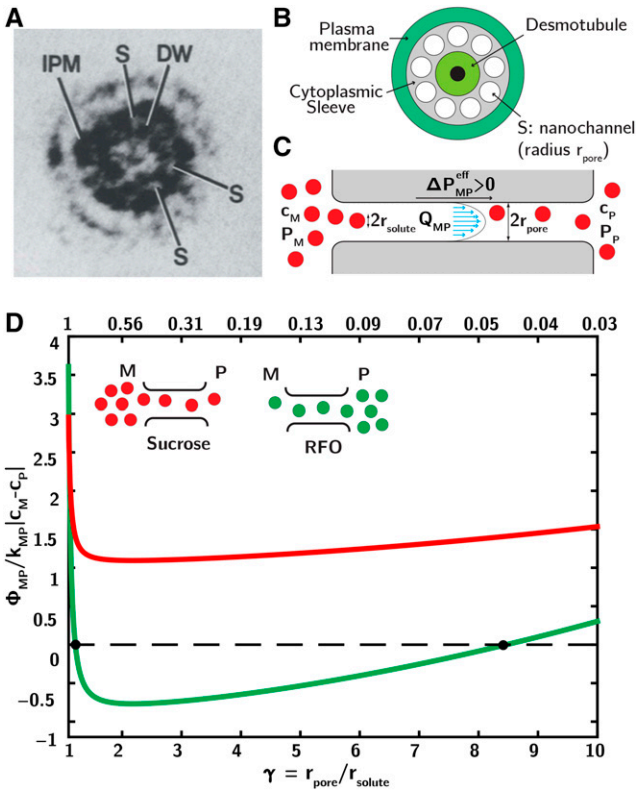

Figure 2. Plasmodesmata transport. A, Transmission electron micrograph showing a transverse cross section of a plasmodesma between phloem parenchyma cells (Fig. 1A presents longitudinal cross section). Note spaces (S) between particles of the desmotubule wall (DW) and the inner leaflet of the plasma membrane (IPM; Ding et al., 1992). B, Schematic representation of longitudinal cross section of a plasmodesma, showing the desmotubule (a tube of appressed endoplasmic reticulum that extends between the adjacent cells); and the cytoplasmic sleeve between the desmotubule and plasma membrane. Membrane proteins are thought to divide the cytoplasmic sleeve into nanochannels (S) which, though irregular in form, are represented as tubes (inspired by Lucas and Jung-Youn, 2004). C, Schematic representation of longitudinal cross section of a nanochannel. Molecules of hydrodynamic radius r_{solute} are transported by advection (Q_{MP}) and diffusion through a nanochannel of radius r_{pore}. Water flow is created by an effective pressure difference $\Delta P_{MP}^{eff} = \Delta P - \sigma_{suc} RT \Delta c_{suc} - \sigma_{RFO} RT \Delta c_{RFO} > 0$ between mesophyll (M) and phloem (P). D, Ratio of total and diffusive molar fluxes of solute in a channel submitted to an effective pressure difference ΔP_{MP}^{eff} of 0.2 bar ($P_M^{eff} > P_P^{eff}$) across a single channel (not coupled to the global model) as a function of the confinement parameter $\gamma = r_{pore}/r_{solute}$ (bottom axis) or equivalent reflection coefficient, σ_{MP} (top axis; Supplemental Eq. S21). The gradient of solute is either with (red, Suc) or against (green, stachyose) the direction of water flow, with $c_i^{max} = 1.5 \cdot c_i^{min}$. See Supplemental Information S1 for details on the plasmodesmata transport model, and Supplemental Information S3 for estimation of the effective pressure difference.

$$Q_P^c = L_{tot} \Delta P_c = L_{tot} \left[RT c_M^{suc} + P_X - P_S \right] . \qquad (3)$$

This flow carries sugars out of the MV-phloem at a rate, $\phi_P^c = Q_P^c \cdot c_P^{suc} \approx Q_P^c \cdot c_M^{suc}$, so that we expect that the concentration of sugars in the phloem will depend, in part, on a competition between this advective transfer and Suc diffusion from the mesophyll through the plasmodesmata interface. We approximate this diffusive loading flux as $k_{MP}^{suc}(c_M^{suc} - c_P^{suc}) \approx k_{MP}^{suc} c_M^{suc}$, where k_{MP}^{suc} [m s^{-1}] is the diffusive mass transfer coefficient of Suc through the plasmodesmatal interface. To characterize this competition, we propose the following nondimensional ratio of global advection out of the transport phloem and local diffusion through plasmodesmata:

$$f \equiv \frac{\text{advection}}{\text{diffusion}} = \frac{Q_P^c c_M^{suc}}{k_{MP}^{suc} c_M^{suc}} = \frac{Q_P^c}{k_{MP}^{suc}} = \frac{L_{tot}\left[RT c_M^{suc} + P_X - P_S\right]}{k_{MP}^{suc}} . \qquad (4)$$

For large values of this flushing number, f, phloem loading is diffusion limited and the concentration of phloem sugars will be low because sugars are flushed out of the MV-phloem more quickly than they can diffuse in; gradient inversion (elevated total concentration of sugars in MV-phloem; Fig. 1, B and C) is suppressed in this regime. For small values of f, loading is convection limited and sugar concentration in the MV-phloem is high, favoring gradient inversion. This number is relevant for both passive and active symplastic loaders (Comtet et al., 2017).

Physiology of the Plasmodesmata

Although segregation of RFOs based on a size exclusion mechanism has been proposed (Turgeon, 1991; Dölger et al., 2014), discrimination based only on hydrodynamic radii seems difficult considering that stachyose is only 40% larger than Suc (Liesche and Schulz, 2013), and raffinose is even smaller than stachyose. Even if the RFOs mass transfer coefficient is reduced by steric interaction with plasmodesmatal channels (Turgeon and Gowan, 1990; Dölger et al., 2014), back diffusion and leakage of RFOs into the mesophyll will eventually occur. Dölger et al. (2014) presented a physical model of hindered transport of Suc through the plasmodesmata interface, concluding that the reentry of raffinose in the mesophyll could not be prevented by advective sweeping due to water flow through plasmodesmata. Here, we present an explicit model of advection and diffusion within the plasmodesmata (Fig. 2) coupled with our global model of symplastic transport (Fig. 1E) to reexamine the mechanism of RFO segregation.

Pore-Scale Model of Plasmodesmata Transport

Figure 2A presents an electron micrograph of a plasmodesma in transverse section. Sugar molecules are thought to pass through the space between the desmotubule (Fig. 2A, "DW") and the plasma membrane, i.e. the "cytoplasmic sleeve," (Fig. 2A, "IPM"). One common, idealized interpretation of the

cytoplasmic sleeve is that of a series of nanochannels created by regularly arranged proteins within the cytoplasmic sleeve (Fig. 2A, "S"; Ding et al., 1992; Terry and Robards, 1987). In Figure 2B, we model each plasmodesma as a bundle of nine pores of equivalent radius r_{pore} and length l (Terry and Robards 1987). In Figure 2C, we follow Deen (1987) and consider hindered transport of spherical solute molecules in cylindrical pores, accounting for steric interactions of solute molecules with the pore wall. In following this approach, we adopt a confinement parameter, the ratio of pore radius to sugar molecule radius, $\gamma_i = \frac{r_{\mathrm{pore}}}{r_{\mathrm{i}}} \geq 1$, where i is either Suc or RFOs; this parameter controls the partial rejection of sugar species i due to steric interactions with the pore, such that the flux of Suc and RFOs from mesophyll to phloem can be expressed as

$$\phi^i_{\mathrm{MP}} = \left[1 - \sigma^i_{\mathrm{MP}}(\gamma_i)\right] Q_{\mathrm{MP}} \left[c^i_M + \frac{c^i_{\mathrm{M}} - c^i_{\mathrm{P}}}{\exp(\mathrm{Pe}_i) - 1} \right] \qquad (5)$$

where $\sigma^i_{\mathrm{MP}}(\gamma_i)$ [−] is the reflection coefficient that depends only on the ratio γ_i, $\mathrm{Pe}_i = [1 - \sigma^i_{\mathrm{MP}}(\gamma_i)]Q_{\mathrm{MP}}/k^i_{\mathrm{MP}}$ is the Péclet number characterizing the ratio of hindered advection to hindered diffusion in the pore, k^i_{MP} is the mass transfer coefficient that accounts for hindered diffusion of solute, and Q_{MP} is the flux of water between mesophyll and phloem (Deen, 1987; Dechadilok and Deen, 2006; Supplemental Eqs. S18–S21). In the limit of low Péclet number, $\mathrm{Pe}_i \ll 1$, Equation 5 simplifies to $\phi^i_{\mathrm{MP}} = k^i_{\mathrm{MP}}(c^i_{\mathrm{M}} - c^i_{\mathrm{P}}) + [1 - \sigma^i_{\mathrm{MP}}(\gamma_i)]Q_{\mathrm{MP}}\, c^i_M$, for which diffusive and advective flux through plasmodesmata are completely decoupled (Supplemental Eq. S24). This limit, for which advective effects are weak, was used by Dölger et al. (2014) in their model of plasmodesmatal transport.

For clarity, we emphasize that the relative strength of advection and diffusion captured by the Péclet number relates to local transport processes within the pores of the plasmodesmata. On the other hand, the flushing number defined in Equation 4 is the ratio of global advection of sugars within the transport phloem to the diffusive component of transport through the plasmodesmata, from mesophyll to phloem. In Supplemental Information S5, we provide a further discussion of the relationship between these nondimensional parameters.

Steric Hindrance and Advection Can Inhibit Back Diffusion of RFOs

To what degree do diffusion and hindered advection affect flux of Suc and RFO through plasmodesmata? In Figure 2D, we focus on the transport of these solutes across the plasmodesmatal interface. We plot the molar fluxes [mol $\mathrm{m}^{-2}\ \mathrm{s}^{-1}$] of Suc (Fig. 2D, red) and RFO (Fig. 2D, green) through a model pore (Fig. 2C) as a function of the confinement parameter $\gamma_i = \frac{r_{\mathrm{pore}}}{r_{\mathrm{i}}}$ (Eq. 5). We normalize the total sugar flux ϕ_{MP} (Eq. 5) by its diffusive component, $k_{\mathrm{MP}}|\Delta c| > 0$. Positive flux corresponds to net transfer from mesophyll (Fig. 2C, left) to phloem (Fig. 2C, right). The upper axis of Figure 2D represents the reflection coefficient, $\sigma_{\mathrm{MP}}(\gamma)$ (Dechadilok and Deen, 2006) for a given confinement parameter (Supplemental Eq. S21). For these calculations, we impose a fixed effective pressure difference $\Delta P^{\mathrm{eff}}_{\mathrm{MP}} = \Delta P - \sigma_{\mathrm{suc}} RT \Delta c_{\mathrm{suc}} - \sigma_{\mathrm{RFO}} RT \Delta c_{\mathrm{RFO}} =$ 0.2 bar driving a water flow between mesophyll and phloem, with $P^{\mathrm{eff}}_{\mathrm{M}} > P^{\mathrm{eff}}_{\mathrm{P}}$ (Supplemental Eqs. S5a-b and S15; Supplemental Information S3). This effective difference in pressure represents the combined effect of the difference in mechanical pressure and the differences in concentration of the two solutes and depends on plasmodesmatal interface reflection coefficients for Suc and RFOs (Katchalsky and Curran, 1965). With this driving force fixed (to isolate the effect of the plasmodesmatal interface), we evaluate the rate of transfer of sugars by combined hindered advection and diffusion in the presence of flow using Equation 5.

For all degrees of confinement, we predict forward flux of Suc (red curve always above zero in Fig. 2D), as expected given the downhill gradient of both effective pressure and Suc concentration. For RFO, the predicted behavior is more complicated: In the limit of strong confinement ($\gamma \to 1$), we predict forward flux of RFO (red line in Fig. 2D), such that no transfer of RFO back from phloem to mesophyll occurs, despite a higher RFO concentration in the phloem. The RFO will be segregated in the phloem. This effect arises because the pore wall impedes more strongly solute diffusion than solute advection. As $\gamma \to 1$, hindrance of diffusive transport occurs due to the increase in the viscous drag experienced by solute particles, while advection of solute is less hindered, as steric interactions restrict solute to the zone of maximum flow in the center of the pore, where advection is strongest (Fig. 2C; Dechadilok and Deen, 2006). At intermediate degrees of confinement ($1.2 < \gamma < 8$ in this example), net backward transfer of RFOs from phloem to mesophyll can occur, as back diffusion outstrips advection with the forward-moving flow. For larger pores ($\gamma > 8$ in this example), we again predict forward flux of RFO and thus its segregation in the phloem, because advection dominates again in this limit.

In summary, we predict that advection of water can inhibit back diffusion of RFO from phloem to mesophyll in the limits of both strong ($\gamma \to 1$) and weak ($\gamma \gg 1$) confinement within the plasmodesmata. The conclusion of Dölger et al. (2014) that water flow cannot prevent back diffusion of RFO should thus be reevaluated by considering transport over the entire range of Péclet number, as in Equation 5. The small Péclet number limit assumed in their analysis underestimated the effect that advective water flow from mesophyll to phloem has on retarding the movement of RFOs in the opposite direction. In other words, their analysis predicted that an unrealistically large bulk flow was necessary to prevent back diffusion of RFO, compared to

our predictions with the more complete expression in Equation 5. Our analysis thus predicts that advection through the plasmodesmata can aid in creating the segregation and gradient inversion that one observes in active symplastic loaders (Fig. 1B). Thus, one does not need to invoke chemical selectivity within the plasmodesmata in order to explain these observations.

Whole-Plant Transport and Plasmodesmatal Selectivity

Figure 3 presents predictions of our global water transport model (Fig. 1, D and E) with the hindered transport model presented in Figure 2. See Table I for the parameter values used in the model. Figure 3 presents distributions of sugars (Fig. 3A) and carbon export rate (Fig. 3B) with respect to the strength of global convection versus advection (flushing number; f) and confinement parameters ($\gamma_{RFO} = r_{pore}/r_{RFO}$ on left axis; $\gamma_{suc} = r_{pore}/r_{suc}$ on right axis) for a typical polymerization rate (see "Materials and Methods"). We use parameters for stachyose to represent RFO species, with degree of polymerization $n = 2$. We assume here that the permeabilities of the xylem-phloem and xylem-mesophyll interfaces have similar values: $L_{XP} = L_{XM} = 5 \cdot 10^{-14}$ m s^{-1} Pa^{-1}. Note that we find qualitatively similar results—gradient inversion can occur—when taking smaller permeabilities (down to $5 \cdot 10^{-16}$ m s^{-1} Pa^{-1}) for either one or the other interface (see Supplemental Information S4).

The charts in Figure 3C present the calculated concentrations of RFO (green) and Suc (red) in the mesophyll cells (M) and phloem (P) at three points of differing convection (varied by changing transport resistance) and hindrance (varied by changing plasmodesmatal radius). In Figure 3, D to F, we explore trends with polymerization rate and present additional trends for pressure, water potential, and effective pressure difference in Supplemental Information S3 (see Table I for parameter values).

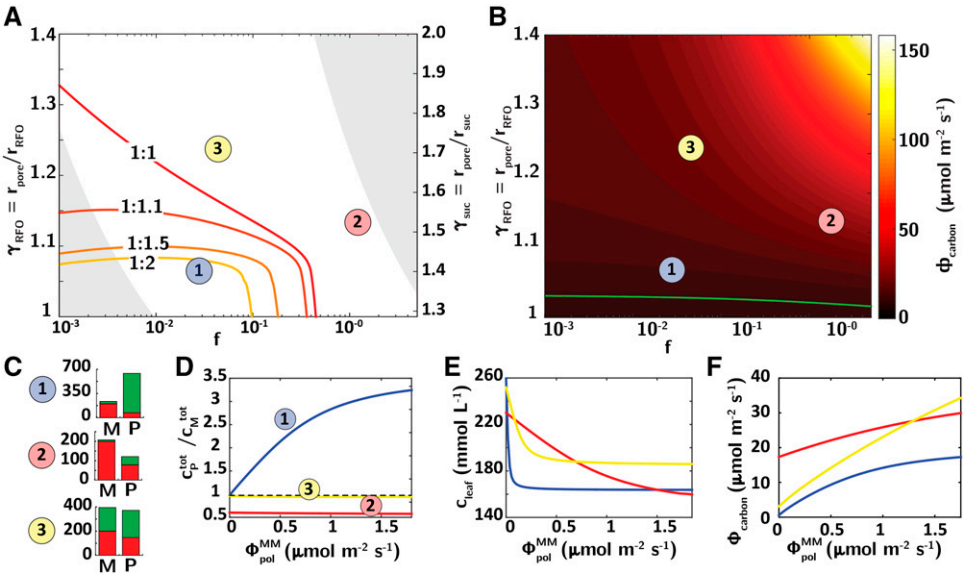

Figure 3. Gradient inversion and export with hindered transport through plasmodesmata. A, State diagram of gradient inversion as a function of confinement parameters, γ_{RFO} and γ_{suc}, and flushing number, f. Isolines show the ratio of the total concentration in the phloem and in the mesophyll, for $r_{stac}/r_{suc} = 1.4$ and hindered plasmodesmatal transport. The red curve (1:1) is the frontier between conditions that provide gradient inversion (minor vein phloem concentration greater than mesophyll concentration, $c_P > c_M$) and those that do not ($c_P < c_M$). The curves 1:1.1, 1:1.5, and 1:2 correspond to 10%, 50%, and 100% excess concentration in the phloem. Point 1, $r_{pore}/r_{RFO} = 1.13$ and $f = 0.04$; point 2, $r_{pore}/r_{RFO} = 1.23$ and $f = 1.4$; point 3, $r_{pore}/r_{RFO} = 1.07$ and $f = 0.02$. In constructing this plot, we varied r_{pore} and L_P keeping other parameters fixed (see "Materials and Methods" and Table I). The gray shaded areas represent conditions outside of the estimated physiological range based on L_p (bottom left boundary, $L_p = 10^{-16}$ m/s/Pa; top right boundary, $L_p = 10^{-12}$ m/s/Pa; Supplemental Eq. S16). We discuss other scenarios in Supplemental Information S4. B, Total translocation rate of equivalent Suc as a function of γ and f. Black, low translocation rates; yellow, high translocation rates. The green line corresponds to a constant export rate of 900 nmol/m^2/s, corresponding to typical physiological values (Schmitz et al., 1987). C, Histograms showing Suc (red) and RFO (green) levels in the mesophyll (M) and phloem (P) for the conditions of the three points indicated in A and B. D to F, Plots of ratio of total concentration in the phloem over total concentration in the mesophyll (D); total concentration in the leaf generated for a constant export rate ϕ^{syn}_{carbon} (E) and equivalent carbon flux (F; Eq. 6) for the three points in A and B. Blue line, point 1; red line, point 2; yellow line, point 3. The variation of pressure, water potential and effective pressure difference in mesophyll and phloem are shown in Supplemental Information S3.

Table I. *Table of parameters (see Supplemental Information S5 for parameter estimation)*

Notation	Definition	Typical Values
Concentrations, $\boldsymbol{c}$ [mmol]		
c_M^{suc}	Sucrose concentration in the mesophylls	200 mmol
c_M^{RFO}	RFO concentration in the mesophylls	–
c_P^{suc}	Sucrose concentration in the minor vein phloem	–
c_P^{RFO}	RFO concentration in the minor vein phloem	–
c_P^{tot}	Total concentration of sugars in the mesophylls ($c_P^{tot} = c_P^{suc} + c_P^{RFO}$)	
c_M^{tot}	Total concentration of sugars in the minor vein phloem ($c_M^{tot} = c_M^{suc} + c_M^{RFO}$)	
c_{leaf}	Average concentration of sugars in the leaf ($c_{leaf} = v_M\ c_M^{tot} + v_P\ c_P^{tot}$)	
Permeabilities, $\boldsymbol{L}$ [m/s/Pa]		
L_{XM}	Xylem/mesophyll permeability (Jensen et al., 2011)	$5{\cdot}10^{-14}$ m s^{-1} Pa^{-1}
L_{XP}	Xylem/phloem permeability (Jensen et al., 2011)	$5{\cdot}10^{-14}$ m s^{-1} Pa^{-1}
L_{MP}	Mesophyll/phloem plasmodesmatal permeability	10^{-13} to $5{\cdot}10^{-12}$ m s^{-1} Pa^{-1}
L_P	Transport phloem equivalent permeability	10^{-10} to 10^{-16} m s^{-1} Pa^{-1}
Pressures and water potentials, $\boldsymbol{P}$ [bar]		
P_X	Xylem water pressure	−1 bar
P_S	Sink (roots) water pressure	0 bar
P_M	Mesophyll hydrostatic pressure	–
P_P	Minor veins hydrostatic pressure	–
Water flux, $\boldsymbol{Q}$ [m/s]		
Q_{XM}	Water flux from xylem to mesophylls	–
Q_{XP}	Water flux from xylem to minor vein phloem	–
Q_{MP}	Plasmodesmatal water flux from mesophylls to phloem	–
Q_P	Water flux through the transport phloem	–
Sugar flux through plasmodesmata, ϕ [mmol/m^2/s]		
ϕ_{MP}^{suc}	Sucrose flux through the plasmodesmata	–
ϕ_{MP}^{RFO}	RFO flux through the plasmodesmata	–
ϕ_{carbon}	Carbon flux transported through the phloem (Eq. 6)	
ϕ_{carbon}^{syn}	Photosynthetic synthetic rate in the mesophyll, equal to the carbon flux exported through the phloem at steady-state (Schmitz et al., 1987)	10.8 μmol m^{-2} s^{-1}
Enzyme kinetics		
ϕ_{pol}	Polymerization rate of sucrose into RFO [mol/m^2/s]	–
ϕ_{pol}^{MM}	Michaelis-Menten maximal rate [mol/m^2/s]	900 nmol m^{-2} s^{-1}
K_M	Michaelis-Menten constant	50 mmol
Plasmodesmatal transport parameters		
D_{suc}	Cytosolic sucrose diffusion coefficient [m^2/s] (Henrion, 1964)	2.3 10^{-10} m^2 s^{-1}
D_{RFO}	Cytosolic RFO diffusion coefficient [m^2/s] (Craig and Pulley, 1962)	1.9 10^{-10} m^2 s^{-1}
$k_D^{suc/RFO}$	Sucrose/RFO plasmodesmatal mass transfer coefficient [m/s]	
$\sigma_{suc/RFO}$	Sucrose/RFO reflection coefficient [−]	0–1
$H_{suc/RFO}$	Sucrose/RFO diffusive hindrance [−]	0–1
$W_{suc/RFO}$	Sucrose/RFO convective hindrance ($W=1-\sigma$) [−]	0–1
ρ	Plasmodesmatal density [m^{-2}] (Gamalei, 1991; Schmitz et al., 1987)	50 μm^{-2}
N	Number of pores per plamodesmata (Terry and Robards, 1987)	9
r_{pore}	pore radius [m] (Schmitz et al., 1987)	0.7–1.5 nm
l_{pore}	pore length [m] (Liesche and Schulz, 2013)	140 nm
r_{suc}	sucrose radius [m] (Liesche and Schulz, 2013)	0.42 nm
r_{RFO}	Stachyose/RFO radius [m] (Liesche and Schulz, 2013)	0.6 nm
$\gamma_{suc} = r_{pore}/r_{suc}$	Sucrose confinement parameter	1–10 in Fig. 2 1.3–2 in Fig. 3
$\gamma_{RFO} = r_{pore}/r_{RFO}$	RFO confinement parameter	1–10 in Fig. 2 1–1.4 in Fig. 3
η_e	Effective phloem sap viscosity including the effects for sieve plates (Jensen et al., 2012)	5 cPs
η_c	Typical cytoplasmic viscosity	2 cPs
Global physiological parameters		
v_M	Volume fraction of mesophyll is the leaf (Adams et al., 2013)	97%
v_P	Volume fraction of phloem in the leaf (Adams et al., 2013)	3%
a	Sieve tube radius [m]	5–20 μm
l_{load}	Length of the loading zone (leaf length) [m]	1–50 cm
h	Length of the transport zone (plant height) [m]	0.1–10 m

Gradient Inversion without Chemically Selective Plasmodesmata

The solid red line in Figure 3A ("1:1") represents the boundary between the states that show gradient inversion and those that do not: Below this curve, for lower γ_{RFO} and γ_{suc} (more restricted motion of sugars within the plasmodesmata) and lower flushing number (i.e. weak global convection and low transport phloem permeability), the total concentration of sugars in the phloem is higher than in the mesophyll. The other curves represent states with excess concentrations of sugar in the phloem relative to the mesophyll. Importantly, for parameters within the physiological range (Fig. 3A, unshaded area), we predict that inversion can occur, with magnitudes of excess concentration in the phloem (Fig. 3A, 50%–100%, point 1 on the diagram) that match those observed in active symplastic loaders (Rennie and Turgeon, 2009). This gradient inversion depends on two conditions: (1) strong geometric confinement within the plasmodesmata ($\gamma_{RFO} < 1.3$; i.e. small plasmodesmatal radius), for which advection of RFO in the plasmodesmata from mesophyll to phloem tends to overcome its back diffusion, corresponding to the limit of $\gamma \to 1$ on the solid green curve in Figure 2B; and (2) weak advection through the phloem (low f, i.e. low transport phloem permeability). If either of these conditions is violated, gradient inversion fails to occur. With strong hindrance and strong global advection (Fig. 3A, point 2), segregation of RFO occurs (green bars in Fig. 3C, point 2), but sugars are flushed out of the phloem, prohibiting gradient inversion. With weak hindrance and weak advection (Fig. 3A, point 3), segregation of RFO does not occur and the gradient between the mesophyll and the phloem tends to zero (Fig. 3C, point 3).

In Figure 3D, we plot the ratio of the total concentrations of sugar ($c^{tot} = c^{suc} + c^{RFO}$) in the phloem and mesophyll for a fixed mesophyll Suc concentration. We associate values of $c_P^{tot}/c_M^{tot} > 1$ with gradient inversion (above the dashed line in Figure 3D). We see that, for weak global advection (low f, i.e. low transport phloem permeability) and hindered transport through plasmodesmata ($\gamma_{RFO} \to 1$, i.e. small plasmodesmatal radius; point 1, blue curve in Fig. 3D), the strength of gradient inversion grows monotonically with polymerization rate, confirming that an increase in diffusive flux created by the Suc depletion in the phloem increases phloem osmolarity, despite the loss of particles through polymerization. For flushing numbers greater than one (Fig. 3D, point 2, red curve) or weak segregation (Fig. 3D, point 3, yellow curve) gradient inversion is never obtained, even for large polymerization rates.

Export Rates Are Compatible with Those Observed Experimentally

We now track the flux of carbon out of leaves expressed, no matter its chemical form, as total moles of carbon (ϕ_{carbon}); Based on the predictions in Figure 3A, the experimentally observed degree of gradient inversion (higher sugar concentration in the phloem) requires strongly hindered transport through the plasmodesmata (small γ_{RFO} as at point 1). To assess the consequences of hindrance on sugar flux, in Figure 3B we plot the total carbon export rate, ϕ_{carbon}, over the same domain as in Figure 3A.

$$\phi_{carbon} = 12 \cdot Q_P \left(c_P^{suc} + n c_P^{RFO} \right) \quad (6)$$

Note that this flux equals the flux of Suc through the plasmodesmatal interface times the carbon content of one Suc. molecule. The green curve in Figure 3B is the isoline for an export rate, $\phi_{carbon}^{syn} = 10.8\ \mu mol\ m^{-2}\ s^{-1}$ corresponding to a typical flux through minor veins (Schmitz et al., 1987; Haritatos et al., 1996). Importantly, the model is consistent with experiments in that strong gradient inversion occurs in a regime that provides physiologically reasonable export rates (as at point 1, Fig. 3B). However, maintaining gradient inversion significantly constrains export rates compared to those given by larger plasmodesmatal pores (point 3, Fig. 3B). This supports the concept that the elevated density of plasmodesmata observed in active symplastic loaders relative to passive ones evolved to accommodate the limitation on flux imposed by the narrow pores required for gradient inversion (Haritatos and Turgeon, 1995; Slewinski et al., 2013). Moreover, the fact that the export rate isoline (green line, Fig. 3B) crosses domains corresponding to various levels of segregation and to the absence of segregation (left and right of the 1:1 isoline, Fig. 3A) suggests that segregation of RFOs and gradient inversion do not provide a direct advantage with respect to export rates, compared to the situation where RFOs leak back to the mesophyll cells.

Polymerization Lowers the Required Concentration of Sugars in the Leaf

We now explore the impact of polymerization on total sugar concentration in the leaf for a fixed rate of synthesis in the mesophyll, ϕ_{carbon}^{syn}, or total carbon export through the phloem (these rates are equal in moles of carbon at steady state). In Figure 3E, we track the average concentration of sugars in the leaf, $c_{leaf} = v_M\, c_M^{tot} + v_P\, c_P^{tot}$, as a function of the rate of polymerization, ϕ_{pol}^{MM}, for the three cases highlighted in Figure 3, A to C. In the definition of c_{leaf}, v_M and v_P are the volume fractions of mesophyll and phloem in a typical leaf. The values of c_{leaf} in the absence of polymerization ($\phi_{pol}^{MM} = 0$) correspond to passive loading. Importantly, Figure 3E shows that the average concentration of leaf sugars required to drive export always decreases with increasing polymerization rate in the MV-phloem. To maintain a given carbon flux, the difference in Suc concentration must be maintained at a fixed value to drive diffusion; increasing the rate of polymerization lowers the phloem Suc concentration and allows the concentration in the mesophyll to drop while maintaining a fixed gradient. Due to the

stoichiometry of polymerization and the small volume fraction occupied by the phloem ($v_P \ll 1$), the RFOs produced contribute negligibly to total leaf sugar content, even in the absence of segregation (point 3, blue curve in Fig. 3E). This prediction supports the hypothesis that polymerization provides a selective advantage by reducing phloem Suc, thus allowing the total sugar concentration in the mesophyll to be maintained at a low level, which in turn increases growth potential and may minimize herbivory (Rennie and Turgeon 2009; Turgeon 2010a).

Increased Polymerization and Phloem Advection Increase Export Rate

We now ask how polymerization and advection in the phloem impact export rate with a fixed concentration of Suc in the mesophyll. For a fixed mesophyll Suc concentration, the exported carbon flux (Eq. 6) always increases with polymerization rate in the MV-phloem (Fig. 3F). This effect is due to the increased gradient in Suc concentration created by Suc depletion in the phloem by polymerization. Figure 3F also shows that export rate increases with decreasing transport phloem resistance, leading to increasing convection (higher *f*, comparing point 1, blue curve, and point 2, red curve). We note that the favorable dependence of translocation rate on polymerization holds only if RFO synthesis is spatially confined to the phloem, because the reaction must selectively decrease the concentration of Suc in the phloem to increase the gradient between the two cellular domains. Also note that the localization of the polymerization reactions within the MV-phloem should not be confused with the spatial localization of the RFO products, which we refer to as "segregation." Confinement of the polymerization reaction enzymes to the companion (intermediary) cells of the phloem has been reported for active symplastic loaders (Holthaus and Schmitz 1991; Beebe and Turgeon 1992).

Polymerization and Segregation Minimize Leaf Sugar Content

We now explore the possible advantages derived from the polymer trap phenomenon (Fig. 3, D–F). Note that an increased rate of polymerization lowers the total sugar concentration in the leaf (c_{leaf}; Fig. 3E) and increases the total carbon export out of the leaf (ϕ_{carbon}; Fig. 3F) regardless of the degree of gradient inversion (Fig. 3D). The notable distinction of the strongly hindered case (point 1, blue curves in Fig. 3, D–F) is that it displays both strong gradient inversion and a rapid decay of c_{leaf} with ϕ_{pol}^{MM}; in leaves operating under these conditions, a small expenditure of metabolic activity dedicated to polymerization will dramatically decrease its load of sugar. This trend suggests that maintaining low sugar content in leaves provides a selective advantage for the evolution of specialized plasmodesmata that enable segregation and gradient inversion in active symplastic loaders.

DISCUSSION

The physical and chemical mechanisms that lead to segregation of RFOs in the phloem of "polymer trap" species are still matters of debate, as are the adaptive advantages of this segregation. To shed light on these topics and on symplastic loading more generally, we have introduced a model that couples local and global transport processes with the polymerization kinetics of Suc into RFOs.

Our predictions indicate that, regardless of global hydraulic conditions, localized polymerization of Suc into RFOs in the MV-phloem decreases the total concentration of sugars required in the leaf to export Suc at a fixed rate (Fig. 3E) and increases the rate of export for a fixed concentration of Suc in the mesophyll (Fig. 3F); both of these trends could be beneficial to the plant and provide a basis for a selective pressure toward this metabolically active reaction (Turgeon, 2010a). With the introduction of a simple but complete model of hindered advection and diffusion within the plasmodesmata, we find that the conditions required to provide segregation and gradient inversion lead to physiologically reasonable rates of export, if account is taken for the unusually high density of plasmodesmata at the interface between bundle sheath and intermediary cells (mesophyll/phloem interface) in active symplastic loaders (trapper species). While even higher export rates could be achieved in conditions that do not provide gradient inversion (larger pore radii and higher flushing number), these conditions do not lead to as large a reduction of sugar concentration in the mesophyll as the strongly segregated case (Fig. 3E).

Taken together, our observations are consistent with the hypothesis that the specialized plasmodesmata found in active symplastic loaders—with high density per unit area and nanometer-scale effective pore radii—evolved to provide an adequate export rate (e.g. a value limited by photosynthetic rates) under the additional constraint of minimizing the total sugar content of leaves (Fig. 1C; Rennie and Turgeon, 2009). It has been argued that reducing total carbohydrate concentration in leaves could increase growth potential and limit herbivory (Turgeon, 2010a). We also note that minimizing total sugar concentration in the mesophyll could minimize possible inhibition of photosynthesis (Adams et al., 2013). A clear prediction of the model is that, if selectivity is the result of hindered plasmodesmatal transport, reducing convective flow through plasmodesmata between the bundle sheath and intermediary cells (mesophyll/phloem interface) will impede segregation, leading to accumulation of RFOs in the mesophyll. Along with dye-coupling approaches (Liesche and Schulz, 2012), experiments decreasing the flushing number (by applying cold or girdling the

transport phloem), could give additional insight into potential RFO segregation mechanisms.

Interestingly, most, if not all, symplastic loaders polymerize some Suc into RFOs whether or not they display the gradient inversion associated with polymer trapping (Slewinski et al., 2013). Our model provides a possible rational for this observation: With or without segregation and gradient inversion, localized reduction of Suc in the phloem by polymerization increases export rates relative to the completely passive case (as for points 2 and 3 in Fig. 3F). While trapping species appear to use segregation to prioritize low concentrations in the mesophyll, other symplastic loaders may be exploiting this effect to a lesser degree, prioritizing export rate over the minimization of concentration. In other words, we suggest that polymerization may represent an active loading process in a much larger fraction of symplastic loaders than has been previously appreciated. It would be interesting to confirm the predicted relation between polymerization and translocation experimentally by genetically enhancing or inhibiting polymerization rates in both symplastic loaders that show gradient inversion and those that do not (Cao et al., 2013; McCaskill and Turgeon, 2007). Such techniques could potentially play a role in improving phloem export rates and yields in symplastic loaders.

Finally, we note that apoplastic loading could theoretically occur in parallel with active and passive symplastic loading mechanisms, either in the same or in different cells. However, available evidence does not support the presence of complementary apoplastic and symplastic mechanisms in intermediary cells: The Suc transporter does not immunolocalize to the intermediary cell plasma membrane (Voitsekhovskaja et al., 2009). It is possible, even likely, that apoplastic loading occurs in other companion cells in RFO plants (those that do not express the RFO pathway), but if so this contribution is apparently minimal since blocking the Suc transporter chemically (Turgeon and Gowan, 1990) or by RNAi (Zhang and Turgeon, 2009) does not noticeably inhibit growth. Nonetheless, the effect of additional Suc flux at the mesophyll/phloem interface due to apoplastic loading could be implemented in the model. These issues will be addressed in future studies.

Our study allowed us to characterize the flow patterns arising from coupled water and solute transport in leaf phloem, when water is allowed to flow through plasmodesmata. Importantly, in the presence of gradient inversion, we found that water always flows advectively from mesophyll to phloem, even when there exists an adverse gradient in both hydrostatic pressure and water potential (Supplemental Information S3; gradient inversion leads to larger pressure and water potential in the phloem than in the mesophyll). This effect arises due to the properties of the plasmodesmatal interface—partially reflective to both Suc and RFOs—for which an effective pressure difference, $\Delta P_{\mathrm{eff}} = \Delta P_{\mathrm{MP}} - RT[\sigma^{\mathrm{suc}}\Delta c^{\mathrm{suc}}_{\mathrm{MP}} + \sigma^{\mathrm{RFO}}\Delta c^{\mathrm{RFO}}_{\mathrm{MP}}]$, provides the driving force for advective water flow, Q_{MP} (Katchalsky and Curran, 1965). We note that this pressure difference is distinct from either the differences in water potential or in hydrostatic pressure. Indeed, because the small dimensions of the plasmodesmatal channels lead to a larger reflection coefficient for RFOs than for Suc, the uphill gradient of RFOs ultimately provides the dominant force that induces advective water flow from mesophyll to phloem.

Our model of transport through plasmodesmata shows that both segregation of RFOs in the phloem and gradient inversion can occur without strict steric exclusion or chemical selectivity (Fig. 3A). We conclude that convective sweeping of RFOs downstream in the plasmodesmata (from mesophyll to phloem) plays a critical role in driving these effects, in contrast to the conclusions of a recent study (Dölger et al., 2014). We do not exclude the possibility that molecular mechanisms (e.g. due to molecularly specific steric or chemical effects in the pores) could impact the selectivity for transfer of Suc relative to RFOs. We also allow that, as noted by Liesche and Schulz (2013), stachyose diffusing into the mesophyll could be hydrolyzed back into Suc and monosaccharides by the α-galactosidase present in mature leaves, preventing stachyose accumulation in the mesophyll. To clarify this mechanism further will require additional information on sugar gradients, hydraulic coupling between mesophyll and phloem (Voitsekhovskaja et al., 2006), and the structure and biochemistry of the pore spaces within plasmodesmata; additionally, more detailed models of molecular transport under strong confinement should be employed (Bosi et al., 2012). Our model provides a framework in which to evaluate the impact of these details on the global characteristics of the loading process.

In conclusion, our study highlights the impact of system-scale coupling on the dynamics of symplastic loading and sheds light on the possible selective advantages derived from the polymerization and segregation that are observed in polymer trap species. We propose that evolutionary drivers other than increased export rate should be sought to explain sugar segregation in active symplastic loaders and that up-regulation of the enzymatic pathways that synthesize RFO could lead to improved export rates in passive symplastic loaders. In conjunction with future experiments, refinements of this model could provide a basis for directing the design of engineered plants with more efficient translocation of sugars, faster growth, and higher yields.

MATERIALS AND METHODS

Boundary Condition for Mesophyll Suc

Photosynthesized carbohydrates can selectively be stored as starch or Suc. This partitioning led us to consider, in Figure 3, two extreme boundary conditions for the export and concentration of mesophyll Suc. When photosynthesis is not limiting, we consider Suc concentration to be fixed at 200 mM in the mesophyll (Fig. 3, A–D and F). For limiting photosynthesis, all sugars are exported and a fixed carbon flux $\phi^{\mathrm{syn}}_{\mathrm{carbon}} = 10.8\ \mu\mathrm{mol\ m^{-2}\ s^{-1}}$ has to be

accommodated through the phloem (Schmitz et al., 1987; Haritatos et al., 1996; Fig. 3E; see Supplemental Information S1 and Supplemental Eq. S11 for more details).

Coupling to the Xylem

Windt et al. (2006) showed experimentally that the impact of phloem flow on xylem water status is weak. We thus take fixed water pressure in the xylem, $P_X = -0.1$ MPa, to represent leaves at moderate stress. Change in xylem water potential would simply shift the flushing number f. Mesophyll cells and minor veins are surrounded by cell walls, which, as part of the apoplast, can lead to direct hydraulic coupling to the xylem. Due to differences in water potential, water from the xylem can enter these cells via osmosis through membrane aquaporins (Fig. 1, D and E, blue arrows; Patrick et al., 2001). In Figure 3, we take the equivalent water permeability of these interfaces to be $L_{XP} = L_{XM} = 5 \cdot 10^{-14}$ m s^{-1} Pa^{-1} (Thompson and Holbrook, 2003; the effect of different permeabilities is presented in Supplemental Information S4).

Enzyme Kinetics

We assume segregation of the enzymes in the minor veins and assume that the enzyme-mediated polymerization follows Michaelis-Menten kinetics with a maximal polymerization rate ϕ_{pol}^{MM} (Fig. 3, E and F), and $K_m = 50$ mmol (Supplemental Eq. S16). In Figure 3, A and B, we take $\phi_{pol}^{MM} = 900$ nmol m^{-2} s^{-1} (the typical export rate of Suc in polymer trappers; Schmitz et al., 1987).

Sink Kinetics

We take pressure in the phloem sap at the sinks, $P_S = 0$ MPa; this choice is equivalent to neglecting rate limitations at the unloading step, but variations of the unloading rate can be accounted for by varying the conductance of the transport phloem, L_P.

Plasmodesmatal Interface and Sugar Filtering

We assume a density of 50 plasmodesmata/μm^2 of cell wall at the bundle sheath-intermediary cells interface (Schmitz et al., 1987; Gamalei, 1991). We take pore-length of 140 nm, equal to half of the total wall thickness (Volk et al., 1996), corresponding to the length of the branched side of the plasmodesmata, as this section of the passage is more constricted and will thus dominate both hydraulic resistance and transport selectivity. We treat each plasmodesma as a bundle of $n = 9$ pores (Fig. 2A; Terry and Robards, 1987). For solute hydrodynamic radius, we calculated values from 3D hydrated models of Suc (r_{suc} = 0.42 nm) and stachyose (r_{stac} = 0.6 nm; Liesche and Schulz, 2013). We vary plasmodesmata pore size between r_{pore} = 0.6 nm and 0.84 nm in Figure 3.

General Modeling Hypothesis

We assume throughout our model that all the supracellular compartments are well mixed. Phloem sap viscosity can be affected by the relative sugar content and concentration (Hölttä et al., 2006; Lang, 1978; Jensen et al., 2013), but we neglect this effect by considering a hydraulic permeability L_P independent of sap composition. The physiological values above and in Table I are of the right order of magnitude and provide a basis for exploring trends, via changes of the nondimensional flushing number, f (changing the transport phloem hydraulic permeability L_P), reaction rate, ϕ_{pol}^{MM}, and confinement parameter γ (changing plasmodesmatal pore size r_{pore}). At steady state, our model provides fourteen equations (Supplemental Eqs. S1–S14) that we solve for the fourteen unknown pressures, concentrations, and fluxes shown in blue and red in Figure 1E (Supplemental Information S1).

Supplemental Data

The following supplemental materials are available.

Supplemental Figure S1. Labeled electron micrograph corresponding to the model of Figure 1D.

Supplemental Figure S2. Concentration profile inside the plasmodesmatal pore.

Supplemental Figure S3. Effect of xylem to phloem and xylem to mesophyll permeabilities on segregation levels.

Supplemental Figure S4. Details of hydrostatic pressures, water potentials, and effective pressure differences for the three scenarios of Figure 3.

Supplemental Figure S5. Ratio of RFO and sucrose Peclet numbers as a function of the confinement parameter and plasmodesmatal pore radius.

Supplemental Information S1. Mathematical treatment.

Supplemental Information S2. Relationship between local plasmodesmatal transport and flushing number.

Supplemental Information S3. Pressure, water potential, and effective pressure difference in mesophyll and phloem.

Supplemental Information S4. An alternative scenario for water transport.

Supplemental Information S5. Parameter estimation.

ACKNOWLEDGMENTS

We thank Kaare Jensen for fruitful discussions and one anonymous reviewer for insightful comments.

Received July 6, 2016; accepted July 28, 2017; published August 9, 2017.

LITERATURE CITED

Adams III WW, Muller O, Cohu CM, Demmig-Adams B (2013) May photoinhibition be a consequence, rather than a cause, of limited plant productivity? Photosynth Res **117:** 31–44

Beebe DU, Turgeon R (1992) Localization of galactinol, raffinose, and stachyose synthesis in *Cucurbita pepo leaves.* Planta **188:** 354–361

Bosi L, Ghosh PK, Marchesoni F (2012) Analytical estimates of free brownian diffusion times in corrugated narrow channels. J Chem Phys **137:** 174110

Cao T, Lahiri I, Singh V, Louis J, Shah J, Ayre BG (2013) Metabolic engineering of raffinose-family oligosaccharides in the phloem reveals alterations in carbon partitioning and enhances resistance to green peach aphid. Front Plant Sci **4:** 263

Comtet J, Jensen KH, Turgeon R, Stroock AD, Hosoi AE (2017) Passive phloem loading and long-distance transport in a synthetic tree-on-a-chip. Nat Plants **3:** 17032

Dechadilok P, Deen WM (2006) Hindrance factors for diffusion and convection in pores. Ind Eng Chem Res **45:** 6953–6959

Deen WM (1987) Hindered transport of large molecules in liquid-filled pores. AIChE J **33:** 1409–1425

Ding B, Turgeon R, Parthasarathy MV (1992) Substructure of freeze-substituted plasmodesmata. Protoplasma **169:** 28–41

Dölger J, Rademaker H, Liesche J, Schulz A, Bohr T (2014) Diffusion and bulk flow in phloem loading: A theoretical analysis of the polymer trap mechanism for sugar transport in plants. Phys Rev E Stat Nonlin Soft Matter Phys **90:** 042704

Fisher DG (1986) Ultrastructure, plasmodesmatal frequency, and solute concentration in green areas of variegated *Coleus blumei* Benth. leaves. Planta **169:** 141–152

Fu Q, Cheng L, Guo Y, Turgeon R (2011) Phloem loading strategies and water relations in trees and herbaceous plants. Plant Physiol **157:** 1518–1527

Gamalei Y (1991) Phloem loading and its development related to plant evolution from trees to herbs. Trees (Berl West) **5:** 50–64

Giraldo JP, Landry MP, Faltermeier SM, McNicholas TP, Iverson NM, Boghossian AA, Reuel NF, Hilmer AJ, Sen F, Brew JA, et al (2014) Plant nanobionics approach to augment photosynthesis and biochemical sensing. Nat Mater **13:** 400–408

Haritatos E, Keller F, Turgeon R (1996) Raffinose oligosaccharide concentrations measured in individual cell and tissue types in *Cucumis melo* L. leaves: Implications for phloem loading. Planta **198:** 614–622

Haritatos E, Turgeon R (1995) Symplastic phloem loading by polymer trapping. *In* HG Pontis, GL Salerno, EJ Echeverria, eds, Sucrose Metabolism, Biochemistry, Physiology and Molecular Biology. Amer Soc Plant Physiol, Rockville, MD, pp 216–224.

Henrion PN (1964) Diffusion of sucrose in some three-component aqueous solutions. Trans Faraday Soc **60:** 75–82

Holthaus U, Schmitz K (1991) Distribution and immunolocalization of stachyose synthase in *Cucumis melo* L. Planta **185:** 479–486

Hölttä T, Vesala T, Sevanto S, Perämäki M, Nikinmaa E (2006) Modeling xylem and phloem water flows in trees according to cohesion theory and Münch hypothesis. Trees (Berl West) **20:** 67–78

Jensen KH, Lee J, Bohr T, Bruus H, Holbrook NM, Zwieniecki MA (2011) Optimality of the Münch mechanism for translocation of sugars in plants. J R Soc Interface **8:** 1155–1165

Jensen KH, Liesche J, Bohr T, Schulz A (2012) Universality of phloem transport in seed plants. Plant Cell Environ **35:** 1065–1076

Jensen KH, Savage JA, Holbrook NM (2013) Optimal concentration for sugar transport in plants. J R Soc Interface **10:** 20130055

Jensen KH, Zwieniecki MA (2013) Physical limits to leaf size in tall trees. Phys Rev Lett **110:** 018104

Katchalsky A, Curran PF (1965) Nonequilibrium Thermodynamics in Biophysics. Harvard University Press, Cambridge, MA

Knoblauch M, Peters WS (2010) Münch, morphology, microfluidics—our structural problem with the phloem. Plant Cell Environ **33:** 1439–1452

Lacointe A, Minchin PEH (2008) Modelling phloem and xylem transport within a complex architecture. Funct Plant Biol **35:** 772–780

Lang A (1978) A model of mass flow in the phloem. Funct Plant Biol **5:** 535–546

Liesche J, Schulz A (2012) In vivo quantification of cell coupling in plants with different phloem-loading strategies. Plant Physiol **159:** 355–365

Liesche J, Schulz A (2013) Modeling the parameters for plasmodesmal sugar filtering in active symplasmic phloem loaders. Front Plant Sci **4:** 207

Lucas WJ, Jung-Youn L (2004) Plasmodesmata as a supracellular control network in plants. Nat Rev Mol Cell Biol **5:** 712

McCaskill A, Turgeon R (2007) Phloem loading in *Verbascum phoeniceum* L. depends on the synthesis of raffinose-family oligosaccharides. Proc Natl Acad Sci USA **104:** 19619–19624

Münch E (1930) Stoffbewegungen in Der Pflanze. Gustav Fischer Verlag. Jena, Germany

Patrick JW, Zhang WH, Tyerman SD, Offler CE, Walker NA (2001) Role of membrane transport in phloem translocation of assimilates and water. Aust J Plant Physiol **28:** 695–707

Rennie EA, Turgeon R (2009) A comprehensive picture of phloem loading strategies. Proc Natl Acad Sci USA **106:** 14162–14167

Schmitz K, Cuypers B, Moll M (1987) Pathway of assimilate transfer between mesophyll cells and minor veins in leaves of *Cucumis melo* L. Planta **171:** 19–29

Schroeder JI, Delhaize E, Frommer WB, Guerinot ML, Harrison MJ, Herrera-Estrella L, Horie T, Kochian LV, Munns R, Nishizawa NK, et al (2013) Using membrane transporters to improve crops for sustainable food production. Nature **497:** 60–66

Slewinski TL, Zhang C, Turgeon R (2013) Structural and functional heterogeneity in phloem loading and transport. Front Plant Sci **4:** 244

Stroock AD, Pagay VV, Zwieniecki MA, Holbrook NM (2014) The physicochemical hydrodynamics of vascular plants. Annu Rev Fluid Mech **46:** 615–642

Terry BR, Robards AW (1987) Hydrodynamic radius alone governs the mobility of molecules through plasmodesmata. Planta **171:** 145–157

Thompson MV, Holbrook NM (2003) Scaling phloem transport: Water potential equilibrium and osmoregulatory flow. Plant Cell Environ **26:** 1561–1577

Turgeon R (1991) Symplastic phloem loading and the sink-source transition in leaves: A model. *In* J-L Bonnemain, S Delrot, J Dainty, WJ Lucas, eds, Recent Advances in Phloem Transport and Assimilate Compartimentation. Ouest Editions, Nantes, France, pp 18–22

Turgeon R (2010a) The role of phloem loading reconsidered. Plant Physiol **152:** 1817–1823

Turgeon R (2010b) The puzzle of phloem pressure. Plant Physiol **154:** 578–581

Turgeon R, Gowan E (1990) Phloem loading in *Coleus blumei* in the absence of carrier-mediated uptake of export sugar from the apoplast. Plant Physiol **94:** 1244–1249

Voitsekhovskaja OV, Koroleva OA, Batashev DR, Knop C, Tomos AD, Gamalei YV, Heldt HW, Lohaus G (2006) Phloem loading in two Scrophulariaceae species. What can drive symplastic flow via plasmodesmata? Plant Physiol **140:** 383–395

Voitsekhovskaja OV, Rudashevskaya EL, Demchenko KN, Pakhomova MV, Batashev DR, Gamalei YV, Lohaus G, Pawlowski K (2009) Evidence for functional heterogeneity of sieve element-companion cell complexes in minor vein phloem of *Alonsoa meridionalis*. J Exp Bot **60:** 1873–1883

Volk GM, Turgeon R, Beebe DU (1996) Secondary plasmodesmata formation in the minor-vein phloem of *Cucumis Melo* L. and *Cucurbita Pepo* L. Planta **199:** 425–432

Windt CW, Vergeldt FJ, de Jager PA, van As H (2006) MRI of long-distance water transport: A comparison of the phloem and xylem flow characteristics and dynamics in poplar, castor bean, tomato and tobacco. Plant Cell Environ **29:** 1715–1729

Zhang C, Han L, Slewinski TL, Sun J, Zhang J, Wang ZY, Turgeon R (2014) Symplastic phloem loading in poplar. Plant Physiol **166:** 306–313

Zhang C, Turgeon R (2009) Downregulating the sucrose transporter *VpSUT1* in *Verbascum phoeniceum* does not inhibit phloem loading. Proc Natl Acad Sci USA **106:** 18849–18854